The ternary Fe-C-N system: Homogeneous distributions of nitrogen and carbon

Brink, Bastian; Ståhl, Kenny; Christiansen, Thomas Lundin; Somers, Marcel A. J.

Published in:
Journal of Alloys and Compounds

Link to article, DOI:
10.1016/j.jallcom.2016.08.130

Publication date:
2017

Document Version
Peer reviewed version

The ternary Fe-C-N system: Homogeneous distributions of nitrogen and carbon

Bastian K. Brink[a], Kenny Ståhl[b], Thomas L. Christiansen[a], Marcel A. J. Somers[a,*]

[a]Department of Mechanical Engineering, Technical University of Denmark, Produktionstorvet B425, DK-2800 Kgs. Lyngby, Denmark

[b]Department of Chemistry, Technical University of Denmark, Kemitorvet B206, DK-2800 Kgs. Lyngby, Denmark

[*]somers@mek.dtu.dk

Abstract

Porous iron foils were used for synthesizing homogeneous samples of iron carbides and (carbo)nitrides. Homogeneous distributions of interstitial nitrogen and carbon were obtained without long treatment times due to limited required diffusion distances in the porous material. By adjustments of the nitriding and carburizing potentials, tailored nitrogen and carbon contents can be achieved, which allows assessment of a phase stability diagram for the Fe-N-C system, for which available experimental data is limited.

Thermal decomposition sequences were established for the various iron carbides and (carbo)nitrides using *in situ* synchrotron X-ray diffraction. Hägg carbide (χ) and ε-carbonitride, $Fe_2(N,C)_{1-z}$, with high carbon content decompose to cementite (θ) above 850 K, while ferrite (α) forms above 950 K and austenite (γ) above 1025 K. For high nitrogen contents ζ- $Fe_2(N,C)$ is transformed to ε from 680 to 770 K, which decomposes

to γ'-$Fe_4(N,C)_{1+x}$ between 795 and 900 K as nitrogen is released as N_2. Ferrite forms above 850 K while austenite may be briefly formed around 900 K.

The two iron carbides, cementite and Hägg carbide, exhibit different coefficients of thermal expansion. Below approximately 480 K, cementite is ferromagnetic and a volumetric thermal expansion coefficient of $\alpha_V = 1.5 \times 10^{-5}$ K^{-1} is obtained. The average value in the paramagnetic state is $\alpha_V = 4.3\ (2) \times 10^{-5}$ K^{-1}. For Hägg carbide the average value is $\alpha_V = 3.8\ (2) \times 10^{-5}$ K^{-1} and no change as a consequence of a magnetic transition is observed.

Keywords: Nitrocarburizing; iron nitride; iron carbide; phase equilibria

1. Introduction

Nitriding and nitrocarburizing processes introduce atomic nitrogen (N) or both nitrogen and carbon (N + C) into the surface-adjacent region of treated components. The case developing during treatment of iron-based materials typically consists of a compound layer with enhanced wear and tribological performance at the surface, and a diffusion zone underneath, which can enhance fatigue performance. Nitriding is traditionally performed in the temperature range 750 – 800 K, with development of a diffusion zone as the primary purpose, while the main objective of nitrocarburizing is the development of a compound layer, with treatments usually performed at 810 – 860 K [1]. The compound layer typically consists of iron (carbo)nitrides, γ'-$Fe_4(N,C)_{1-x}$ and ε-$Fe_2(N,C)_{1-z}$ but may also contain iron carbides like cementite, Fe_3C [2–5]. The diffusion zone is a

supersaturated interstitial solution of nitrogen (and carbon) in a metallic matrix and alloying element (carbo)nitrides (e.g., CrN and AlN), in the case of alloyed steels.

Currently available experimental data for the phase stability diagram of the Fe–N–C system, as well as isothermal sections of the ternary phase diagram, have been obtained from nitrocarburizing of iron powder in flowing NH_3–H_2–CO gas mixtures [6,7]. The water vapor content in the applied gas mixtures was, however, not provided, implying that the carbon activities in the reported diagrams are ill-determined. The stability of phases in the Fe-N-C system was also inferred from as-grown compound layers on pure iron in NH_3–H_2–CO-N_2 gas mixtures at 853 K [5]; again the carbon activity is undetermined. In such systems a composition gradient occurs over the compound layer and residual stress (gradients) is (are) present. It is doubtful that such systems represent (imposed) equilibrium conditions.

The problem of undetermined carbon activity in the gas phase may be circumvented by using unsaturated hydrocarbons like acetylene (C_2H_2) or propene (C_3H_6), which are potent carburizing agents [8]. Since oxygen is absent, such gasses offer easier thermodynamic control of the gas atmosphere. Also, modified multicomponent gas mixtures have been proposed to independently control the nitriding and carburizing potentials in the gas mixture, albeit with the presence of oxygen [9].

Gaseous processes allow control of the chemical potential of nitrogen and carbon in the gas phase by adjusting the so-called nitriding and carburizing potentials. At 1 atm the nitriding potential is given by $K_N = p(NH_3)/p(H_2)^{3/2}$, where p is the partial pressure expressed in atm. Provided that thermodynamic equilibrium exists between gas and solid phases, the nitrogen activity in the solid state is given by $a_N = K(N)_T \cdot K_N$, where $K(N)_T$ is the temperature-dependent equilibrium constant of the reaction $NH_3 \rightleftharpoons [N] + {}^3/_2\ H_2$ where [N] indicates dissolved nitrogen [10]. Analogously, the carburizing

potential in gaseous mixtures of propene and hydrogen is expressed as $K_C = p(C_3H_6)^{1/3}/p(H_2)$ and $a_C = K(C)_T \cdot K_C$ where $K(C)_T$ is the temperature-dependent equilibrium constant of the reaction $^1/_3C_3H_6 \rightleftharpoons [C] + H_2$ where [C] indicates dissolved carbon [10].

Synthesis of pure and homogeneous specimens of iron nitrides and carbides is practically limited by the diffusion distance of nitrogen/carbon and by the metastability of the compounds with respect to decomposition into iron, graphite (C) and molecular nitrogen (N_2). An imposed equilibrium can be established at the very surface of a specimen in contact with a nitriding or carburizing medium, while elevated temperatures will promote decomposition below the surface. A thin starting material is thus required for the preparation of homogeneous samples.

The surface area of a thin iron foil may be increased by exploiting the metastability of iron nitrides with respect to N_2 at 1 bar [11,12]. As an example, Fig. 1 shows the thermogravimetric curve at 873 K for such a nitriding pretreatment that converts a 25 μm iron foil into porous iron. The initial treatment in gaseous ammonia causes nitrogen to be incorporated throughout the foil until a stationary weight is reached. Away from the surface, nitrogen gas, N_2, develops, which causes the formation of pores throughout the material. The final step, so-called denitriding in a hydrogen atmosphere, completely removes the remaining nitrogen at a considerably higher rate than the initial nitriding, leaving behind a porous iron foil. The resulting (considerably) increased surface area allows an accelerated reaction upon subsequent nitrocarburizing. As the required diffusion distances are shorter, homogeneous samples can be obtained within relatively short time, as compared to the original foil thickness and the samples are stress free. Repeated nitriding and denitriding at a progressively lower temperature leads to an extremely porous foil with a multi-modal distribution of pores that even allows the

subsequent conversion into $Fe_{16}N_2$ at low temperature [13]. In the present work, the simple two-step process was used in order to obtain relatively large pores throughout the material.

Following this pretreatment, the porous iron foils were nitrocarburized in gas mixtures of ammonia, hydrogen and propene adjusted to different combinations of nitriding and carburizing potentials, resulting in the formation of various iron carbides and nitrides. Thermal expansion and phase transformations were studied with *in situ* synchrotron X-ray diffraction.

2. Experimental

Unalloyed 25 μm thick iron foil (99.5% purity, acquired from Advent Research Materials Ltd.) was used for nitrocarburizing with ammonia, nitrogen and hydrogen gasses of 99.999% and propene of 99.5% purity. Both the pretreatment to form porous iron foils and the subsequent nitrocarburizing were performed in ceramic crucibles in a Netzsch STA 449 C Jupiter thermal analyzer. Nitrocarburizing at 718 K was continued until a constant weight was obtained. Total gas flow rates of 58 – 108 mL/min were used including a constant N_2 flow of 5 mL/min for protection of electronics in the measurement compartment. Nitriding (K_N) and carburizing (K_C) potentials, the corresponding activities (a_N and a_C with reference to N_2 and graphite at 1 bar, respectively), treatment time and resulting phase composition for the six samples are given in Table 1. Samples are denoted S1 – S6 and represent a compositional series of progressive increase in nitrogen content and decrease in carbon content. After cooling the porous samples were gently ground to powder in a mortar.

The carbon and nitrogen contents in the samples were determined by combustion infrared detection (carbon content) on a LECO CS230 and by inert gas fusion thermal

conductivity detection (nitrogen content) on a LECO TN500. Since both S4 and S6 contain ζ as a minority phase (see Table 1 and Fig. 2), the composition of ε-phase in these samples was determined assuming the stoichiometric composition, $Fe_2(N,C)_1$, for ζ with a ratio between nitrogen and carbon atoms equal to that of the total sample composition.

Table 1: Nitriding (K_N) and carburizing (K_C) potentials, activities† (a_N and a_C with reference to N_2 and graphite at 1 bar, respectively), required time to reach a stationary weight, carbon and nitrogen content and resulting phase composition.

Sample	S1	S2	S3	S4	S5	S6
K_N [atm$^{-1/2}$]	0.2285	1.468	4.928	17.91	136.6	∞
a_N	30.8	198.1	665.0	2417	18433	∞
K_C [atm$^{-2/3}$]	0.2096	0.6306	1.268	2.835	10.64	∞
a_C	322.4	970.0	1950	4360	16366	∞
Time [hours]	100	94	62	29	8.3	7.7
C [wt %]	6.44	6.22	6.12	3.88	0.96	0.48
N [wt %]	0.09	1.22	2.26	5.97	9.25	10.3
Phases	θ, χ, α	χ, θ, γ', ε	χ, ε	ε, ζ	ε	ε, ζ

†Activities are calculated using thermodynamic data given in references [14] and [15].

X-ray diffractograms were collected at a wavelength of either λ = 1.001952(5) Å or λ = 0.994426(3) Å in transmission mode with a Huber G670 Guinier camera at MAX-lab beamline I711 [16]. In order to reduce the influence of fluorescence, eight aluminum foils (total thickness 160 μm) were positioned in-between the sample and the detector. Samples were either mounted on scotch tape at room temperature or in 0.7 mm inner diameter quartz capillaries filled with an inert argon atmosphere to avoid oxidation on heating in a Huber 670.3 furnace. Temperature calibration and determination of the applied wavelength, as well as correction for diffraction angle (2θ) zero shift, were

performed using a Si standard. For both S1 and S2, 31 diffractograms were measured in the temperature range 413 – 1055 K and for S3 – S6, 22 diffractograms in the range 450 – 1000 K. Data were collected in a 2θ range of 4 – 100° (corresponding to a q range from 0.4 to 9.7 $Å^{-1}$, where $q=4\pi\sin(\theta)/\lambda$) with a fixed step size of 0.005° in 2θ and an exposure time of 240 seconds at each temperature step. After exposure, the temperature was immediately ramped to the next set point (average heating rate of 3 K/min). Rietveld refinements of intensity versus scattering angle (2θ) were carried out using the program *WINPOW*, a local variation of *LHMP* [17] in order to fit lattice parameters and mass fractions of the constituent phases. Pseudo-Voigt profile functions were applied together with Chebyshev background polynomials. Atomic positions were not refined and the following crystal structures were used as initial models for the iron carbides and (carbo)nitrides: θ-Fe_3C [18], χ-Fe_5C_2 [19], γ'-$Fe_4(N,C)_{1-x}$ [20], ε-$Fe_2(N,C)_{1-z}$ [21] and ζ-$Fe_2(N,C)$ [22].

3. Phase composition

X-ray diffractograms for all six samples are shown in Fig. 2. Apart from sample S5, which is monophase, the samples consisted of at least two phases. Remaining ferrite (α) due to incomplete formation of nitrides or carbides was only observed for S1, which was subjected to the lowest nitriding and carburizing potentials and required the longest treatment time to reach a stationary sample weight during nitrocarburizing (Table 1). In addition to ferrite, the sample contained small amounts of Hägg carbide (χ) and the main constituent, cementite (θ). For increasing potentials (S2), formation of Hägg carbide is favored with cementite, γ'-Fe_4N and ε-carbonitride as minor phases. S3 contains only Hägg carbide and ε-carbonitride. Further increase of the nitriding and

carburizing potentials (S3 – S6) leads to formation of ε and ζ phases and drastically reduces the required treatment time.

In the synthesis of iron carbides and nitrides, a combination of low carburizing and low nitriding potentials (low carbon and nitrogen activities) requires relatively long treatment times to reach a stationary sample weight and primarily leads to the formation of iron carbides. Formation of (carbo)nitrides is favored for increasing potentials, which also increase the reaction rate and thus reduce required treatment time, despite the very high carbon activity present. Evidently, for high nitrogen activity in the gas phase, the nitriding reaction dominates. This is in accordance with previous observations on compound layer development on iron during nitrocarburizing [23].

Due to the relatively low X-ray scattering power of nitrogen and carbon, no superstructure reflections yielding direct information on the possible space groups for the ε-phases were observed. Consequently, Rietveld refinements were carried out in space group $P\bar{3}1m$ as reported for ε-$Fe_2(N_{0.8}C_{0.20})_{0.92}$ [21].

4. *In-situ* synchrotron X-ray diffraction

4.1 Phase stability

Phase transformation maps as a function of temperature are given in Fig. 3. The composition of sample S1 is constant up to approximately 850 K where initial decomposition of Hägg carbide (χ) to cementite (θ) is observed. Above 950 K, ferrite (α) is formed, while austenite (γ) forms above 1025 K. Note that, from a mass balance perspective, carbon appears to disappear, because less carbon-rich phases develop from Hägg carbide. It is suggested that this is caused by the formation of graphite. No graphite was detected with X-ray diffraction. This can be ascribed to the high background resulting from diffuse scattering of the capillary or to the development of a

state of carbon, like small domains, that does not diffract X-rays under the given experimental set-up. Similar considerations apply to all samples. For decomposition of the nitrides, nitrogen is released as gaseous N_2.

For S2, the initial primary constituent, Hägg carbide, is transformed to cementite above 850 K, analogous to S1. Thermal decomposition of γ' and ε-phases occurs above 900 K followed by the formation of ferrite and austenite. Both Hägg carbide and ε-carbonitride decompose to cementite above 850 K, followed by the formation of ferrite for S3. No austenite was observed due to the lower final temperature (1000 K) as compared to S1 and S2, where austenite was first observed above 1025 K. Similarly, samples S4 – S6 are composed either entirely of ferrite or in combination with cementite at the final temperature of 1000 K.

For S4 – S6, thermal decomposition of the ζ-phase, if present, is observed from 680 to 770 K while transformation of the ε-carbonitrides occurs between 795 and 900 K. Because of the low carbon content of S5 and S6 (Table 1) no cementite is formed. The nitrogen content is gradually reduced by N_2 release, leading to the formation of γ'-Fe_4N and, eventually ferrite. For S4 and S6, austenite is formed at the same temperature, just below 900 K in excellent agreement with the Fe-N phase diagram [24], where austenite is stabilized by the presence of nitrogen above 865 K. However, this observation seems to contradict the suggestion that austenite would be stable below approximately 850 K in the Fe-N-C system [7,25]. For the carbon-rich samples S1 and S2, austenite is only observed above 1025 K, in accordance with the Fe-C phase diagram [24].

4.2 Expansion coefficients

The mean (volumetric) coefficient of thermal expansion, α_V, for the ε-carbonitrides and for cementite below 480 K was fitted to the expression:

$$V(T) = V_{Tr}[1 + \alpha_V(T\text{-}T_r)] \quad (1)$$

where V is the unit cell volume and V_{Tr} is the volume at a chosen reference temperature, T_r. The unit cell volume of cementite (above 480 K) and of Hägg carbide (for the investigated temperature-range) is preferably described by [26]:

$$V(T) = V_{Tr} \exp\left[\int_{T_r}^{T} \alpha_{exp}(T)dT\right] \quad (2)$$

with the expansion coefficient expressed as $\alpha_V(T) = a_0 + a_1T$. Refined unit cell volumes and fitted expressions for thermal expansion for cementite, Hägg carbide and ε-carbonitrides are presented in Fig. 4. The eventual decrease in unit cell volume for ε, which occurs at lower temperatures for increasing carbon/nitrogen contents, is due to a decrease in interstitial content (i.e. onset of decomposition).

For cementite up to 470 K, a volumetric expansion coefficient of $\alpha_{exp} = 1.5 \times 10^{-5}$ K^{-1} is obtained from Eq. (1). Above this temperature, the expansion coefficient changes as a consequence of a transition from ferromagnetic to paramagnetic cementite. From Eq. (2) the following values were obtained in the temperature range 497 – 1055 K; $a_0 = 2.7$ (1) $\times 10^{-5}$ K^{-1} and $a_1 = 2.0$ (2) $\times 10^{-8}$ K^{-2}. This yields an average of $\alpha_V = 4.3$ (3) $\times 10^{-5}$ K^{-1} in excellent agreement with the value $\alpha_V = 4.1$ (1) $\times 10^{-5}$ K^{-1} obtained by Wood *et al.* [27]. The expansion coefficient of cementite is slightly lower than that of b.c.c. iron, $\alpha_V = 4.4 \times 10^{-5}$ K^{-1} for a similar temperature range [28].

No published data is available for the thermal expansion of Hägg carbide. From Eq. (2) the values $a_0 = 3.1\ (2) \times 10^{-5}\ K^{-1}$ and $a_1 = 1.0\ (3) \times 10^{-8}\ K^{-2}$ are obtained. In the temperature range 413 – 890 K, this corresponds to an average volumetric expansion coefficient of $\alpha_V = 3.8\ (5) \times 10^{-5}\ K^{-1}$, which is slightly lower than for cementite. A magnetic transition is expected at around 520 K [29] for Hägg carbide but only a minor change in unit cell volume is discernible around this temperature compared to that observed at the magnetic transition for cementite. Examining the individual lattice parameters it is found that an indication of a (magnetic) transition at around 520 K is most pronouncedly observed for the shortest lattice parameter, *b*, while *a* and *c* lattice parameters appear less sensitive. The scatter among the temperature dependence of the monoclinic angle (β) obscures any effect of a transformation. Data for the anisotropic thermal expansion, i.e. lattice parameters *a*, *b*, *c* and β versus temperature are presented as supplementary material.

For the ε-phase, the expansion coefficients depend on the interstitial content (Table 2). Both the initial lattice parameters at room temperature and the expansion coefficients increase with increasing total interstitial content. The increase in thermal expansion with increasing interstitial content is consistent with observations for the pure ε-nitrides [30]. From comparison of samples S4 and S5 it appears that in particular nitrogen enhances the lattice parameter *c* and the volumetric expansion coefficient.

Table 2: Lattice parameters (*a* and *c*) at room temperature and volumetric expansion coefficients fitted to equation 1 for ε-iron carbonitrides present in samples S3 - S6.

Sample	S3	S4	S5	S6
	$Fe_2(N_{0.611}C_{0.389})_{0.85}$	$Fe_2(N_{0.569}C_{0.431})_{0.92}$	$Fe_2(N_{0.892}C_{0.108})_{0.92}$	$Fe_2(N_{0.948}C_{0.052})_{0.96}$
a [Å]	4.7655(2)	4.77513(4)	4.77729(5)	4.78556(5)

c [Å]	4.3865(2)	4.38934(4)	4.40799(3)	4.41398(3)
α_v [$\times 10^{-5}$ K^{-1}]	3.67 (4)	4.04 (6)	5.28(13)	5.85(15)

5. Discussion

For imposed equilibrium between the gas phase, with fixed a_N and a_C, and the ternary Fe-N-C solid state, it would be expected that generally only one phase is stable, unless an interdependent combination of two or three of the degrees of freedom, i.e. temperature and activities of N and C (at the chosen pressure), occurs and a two-phase or three-phase equilibrium, respectively, is possible. The intention of the present work was to synthesize mono-phase Fe-N-C samples. The experimental observation that more than one phase is present in most investigated samples at the onset of *in situ* X-ray diffraction analysis, suggests that the intended equilibrium between gas and solid state was not achieved. Nevertheless, the average nitrogen and carbon contents in the samples can be compared with the known Fe-N-C phase diagram to verify consistency with the occurrence of two (or more) phases. Since no isothermal section of the phase diagram at 718 K has been published for the ternary Fe-C-N system, the obtained phase compositions are compared to the isothermal section at 773 K [7]. Inserting the phase compositions given in Table 1 into Fig. 5, it is clearly observed that both samples S1 and S2 contain an additional phase as compared to the expected compositions. The additional occurrences of Hägg carbide in S1 and γ'-(carbo)nitride in S2 suggest that a homogeneous distribution of nitrogen and carbon was not obtained, i.e. composition variations exists in these samples. This coincides with the long treatment time necessary to reach a stationary uptake of nitrogen and carbon under the applied (low) nitriding and carburizing potentials/activities. The expected phase compositions were obtained for samples S3 and S5. Samples S4 and S6 contain ζ-Fe_2(N,C), which does not appear in

the isothermal section at 773 K [7], because of its limited thermal stability. This is consistent with the phase transformation maps in Fig. 3 where ζ-phase has disappeared above 770 K.

The initial transformation of Hägg carbide, which was initially present in samples S1-S3, to cementite (and, most likely, also graphite) is consistently observed at approximately 850 K, regardless of the total sample composition. Complete transformation is obtained between 890 and 927 K, in excellent agreement with the range 893 and 923 K assessed from isothermal sections of the Fe-C-N phase diagram [7]. The sample composition cannot be directly followed through the isothermal sections, because the Hägg-carbide-to-cementite transformation corresponds to a reduction of the total amount of carbon dissolved in carbides. Under the given conditions of temperature and pressure, a mixture of graphite and iron is thermodynamically more favorable than the iron carbides cementite or Hägg carbide. Then, the transformation of Hägg carbide to cementite is likely to be associated with the development of graphite. X-ray diffraction did not allow the direct observation of graphite. Analogously, the iron nitrides are less thermodynamically stable than iron and molecular nitrogen, leading to the release of N_2 at elevated temperature.

Thermodynamically, the Lehrer diagram for the Fe-N system [31] shows the stability of Fe-N phases as a function of temperature and nitrogen activity. Analogously, the experimental procedure pursued here allows the construction of a phase stability diagram for Fe-N-C phases for combinations of nitrogen and carbon activities as a function of temperature. This includes the low-temperature stability region of ζ-Fe_2(N,C) for which experimental data is currently not available. In order to completely map the stability range of Fe-N-C phases, a wider collection of samples with

systematically varied compositions is needed. In addition, smaller temperature steps (and perhaps longer holding times at each temperature) are required.

Recent findings of austenite as a stable phase in the Fe-C-N system between 833 and 853 K [25] agrees with the early work by Naumann and Langenscheid [7] in which an eutectoid temperature of approximately 838 K was suggested. Such findings cannot be confirmed by the current investigation since formation of austenite only occurred above 870 K. It is, however, not unlikely that a (slightly) lower temperature would be observed using smaller temperature steps or longer holding times. The current results are therefore not necessarily in conflict with the eutectoid temperature of 859 K obtained from thermodynamic calculations [32], and agree with the very recently reported range of 853 – 863 K which was experimentally determined on (functionally graded) compound layers [33].

6. Conclusions

Porous iron foils were successfully converted into homogeneous iron carbides and (carbo)nitrides by gaseous nitrocarburizing in NH_3-C_3H_6-H_2 gas mixtures. The nitrogen and carbon activities and corresponding nitrogen and carbon contents in the foils can be tailored to investigate the phase stability of Fe-N-C phases and the thermal expansion coefficients of these phases.

Thermal decomposition of Hägg carbide (χ) and ε-carbonitride with high carbon content (>12 at.%) and relatively low nitrogen content (< 18 at.%) proceeds in the following sequence: $\chi/\varepsilon \rightarrow \theta \rightarrow \alpha \rightarrow \gamma$. Decomposition to cementite (θ) occurs above 850 K. Above 950 K, ferrite (α) is formed and austenite (γ) above 1025 K. The sequential reduction in carbon content is presumably accompanied by graphite

formation although this phase was not directly observed. Excess nitrogen is released as N_2.

For high (> 30 at.%) nitrogen contents the decomposition sequence is: (ζ) → ε → γ' → (γ) → α. If initially present, ζ is transformed into ε in the temperature range 680 - 770 K. Between 795 and 900 K ε decomposes to γ' under the release of N_2. With further reduction of the nitrogen content, ferrite forms above 850 K. Austenite, stabilized by the presence of nitrogen, may be briefly formed below 900 K.

For cementite, a volumetric thermal expansion coefficient of $\alpha_V = 1.5 \times 10^{-5}$ K^{-1} is obtained below approximately 480 K, where this phase is ferromagnetic. In the paramagnetic state above 480 K the average value is $\alpha_V = 4.3\ (3) \times 10^{-5}$ K^{-1}. For Hägg carbide the average value is $\alpha_V = 3.8\ (5) \times 10^{-5}$ K^{-1}. The thermal expansion coefficients obtained for ε-phases are between $\alpha_V = 3.67\ (4) \times 10^{-5}$ K^{-1} and $\alpha_V = 5.85\ (15) \times 10^{-5}$ K^{-1} depending on the interstitial content.

Acknowledgements

The authors are grateful to Danscatt for financing travel expenses in connection with measurement time at MAX-lab. The Danish Council for Independent Research (DFF) is gratefully acknowledged for financial support under Grant 11-106293.

References

[1] M.A.J. Somers, In: G. Krauss (Editor), Comprehensive Materials Processing Vol. 12, Elsevier Ltd., 2014: pp. 413–437.

[2] P.F. Colijn, E.J. Mittemeijer, H.C.F. Rozendaal, Light-microscopical analysis of nitrided or nitrocarburized iron and steels, Z. Metallkd. 74 (1983) 620–627.

[3] M.A.J. Somers, E.J. Mittemeijer, Formation and growth of compound layer on nitrocarburizing iron: Kinetics and microstructural evolution, Surf. Eng. 3 (1987) 123–137.

[4] J. Slycke, L. Sproge, Kinetics of the gaseous nitrocarburising process, Surf. Eng. 5 (1989) 125–140.

[5] T. Woehrle, A. Leineweber, E.J. Mittemeijer, Microstructural and phase evolution of compound layers growing on α-iron during gaseous nitrocarburizing, Metall. Mater. Trans. A. 43 (2012) 2401–2413.

[6] F.K. Naumann, G.L. Langenscheid, Das Aufstickungs- und Aufkohlungsvermoegen von Ammoniak-Kohlenoxyd-Wasserstoff-Gemischen, Arch. Eisenhüttenwes. 36 (1965) 583–590.

[7] F.K. Naumann, G.L. Langenscheid, Beitrag zum System Eisen-Stickstoff-Kohlenstoff, Arch. Eisenhüttenwes. 36 (1965) 677–682.

[8] H. Pedersen, T.L. Christiansen, M.A.J. Somers, Nitrocarburising in ammonia-hydrocarbon gas mixtures, HTM J. Heat Treatm. Mat. 66 (2011) 76–81.

[9] A. Leineweber, T. Gressmann, E.J. Mittemeijer, Simultaneous control of the nitrogen and carbon activities during nitrocarburising of iron, Surf. Coatings Technol. 206 (2012) 2780–2791.

[10] E.J. Mittemeijer, M.A.J. Somers, Thermodynamics, kinetics and process control of nitriding, Surf. Eng. 13 (1997) 483–497.

[11] L. Maldzinski, Z. Przylecki, J. Kunze, Equilibrium between ammonia-hydrogen mixtures and the epsilon-phase of iron, Steel Res. 57 (1986) 645–649.

[12] M.A.J. Somers, N.M. van der Pers, D. Schalkoord, E.J. Mittemeijer, Dependence of the Lattice Parameter of γ' Iron Nitride, Fe_4N_{1-x}, on Nitrogen Content; Accuracy of the Nitrogen Absorption Data, Metall. Mater. Trans. A. 20 (1989) 1533–1539.

[13] T.L. Christiansen, M.A.J. Somers, R.B. Frandsen, Patent application WO 2015/193295 A1, (2015).

[14] J.T. Slycke, E.J. Mittemeijer, M.A.J. Somers, In: E.J. Mittemeijer, M.A.J. Somers (Editors), Thermochemical Surface Engineering of Steels, Woodhead Publishing, Cambridge, UK, 2015: pp. 3–111.

[15] J. Chao, B.J. Zwolinski, Ideal gas thermodynamic properties of ethylene and propylene, J. Phys. Chem. Ref. Data. 4 (1975) 251–261.

[16] Y. Cerenius, K. Ståhl, L.A. Svensson, T. Ursby, A. Oskarsson, J. Albertsson, et al., The crystallography beamline I711 at MAX II, J. Synchrotron Radiat. 7 (2000) 203–8.

[17] R.J. Hill, C.J. Howard, LHPM. A Computer Program for Rietveld Analysis of Fixed-Wavelength X-ray and Neutron Powder Diffraction Patterns, AAEC (Now ANSTO) Rep. M112. (1986) Lucas Heights Research Laboratory, Australia.

[18] F.H. Herbstein, J. Smuts, Comparison of X-ray and neutron-diffraction refinements of the structure of cementite Fe_3C, Acta Crystallogr. 17 (1964) 1331–1332.

[19] A. Leineweber, S. Shang, Z.-K. Liu, M. Widenmeyer, R. Niewa, Crystal structure determination of Hägg carbide, χ-Fe_5C_2 by first-principles calculations and Rietveld refinement, Z. Krist. 227 (2012) 207–220.

[20] H. Jacobs, D. Rechenbach, U. Zachwieja, Structure determination of γ'-Fe_4N and ε-Fe_3N, J. Alloys Compd. 227 (1995) 10 – 17.

[21] A. Leineweber, H. Jacobs, F. Hüning, H. Lueken, W. Kockelmann, Nitrogen ordering and ferromagnetic properties of ε-Fe_3N_{1+x} ($0.10 \leq x \leq 0.39$) and ε-$Fe_3(N_{0.80}C_{0.20})_{1.38}$, J. Alloys Compd. 316 (2001) 21–38.

[22] D. Rechenbach, H. Jacobs, Structure determination of ζ-Fe_2N by neutron and synchrotron powder diffraction, J. Alloys Compd. 235 (1996) 15–22.

[23] M.A.J. Somers, Thermodynamics, kinetics and microstructural evolution of the compound layer; A comparison of the states of knowledge of nitriding and nitrocarburising, Heat Treat. Met. 27 (2000) 92–102.

[24] T.B. Massalski, Binary Alloy Phase Diagrams, 2nd editon: ASM International, 1996.

[25] W.L. Chen, C.L. Wu, Z.R. Liu, S. Ni, Y. Hong, Y. Zhang, et al., Phase transformations in the nitrocarburizing surface of carbon steels revisited by microstructure and property characterizations, Acta Mater. 61 (2013) 3963–3972.

[26] Y. Fei, AGU Reference Shelf 2: Mineral Physics and Crystallography, 1995: pp. 29–44. Washington, DC: AGU.

[27] I.G. Wood, L. Vočadlo, K.S. Knight, D.P. Dobson, W.G. Marshall, G.D. Price, et al., Thermal expansion and crystal structure of cementite, Fe_3C, between 4 and 600 K determined by time-of-flight neutron powder diffraction, J. Appl. Crystallogr. 37 (2004) 82–90.

[28] Z.S. Basinski, W. Hume-Rothery, A.L. Sutton, The Lattice Expansion of Iron, Proc. R. Soc. London A. 229 (1955) 459–467.

[29] L.J.E. Hofer, Nature of the carbides of iron, U.S. Bureau of Mines Bulletin. 631 (1966) 1–60.

[30] A. Leineweber, H. Jacobs, W. Kockelmann, S. Hull, D. Hinz-Hübner, High temperature axial ratios c/a in hcp-based ε-type interstitial nitrides MN_y with M = Mn, Fe, Ni, J. Alloys Compd. 384 (2004) 1–5.

[31] E. Lehrer, Über das Eisen-Wasserstoff-Ammoniak-Gleichgewicht, Z. Elektrochem. 36 (1930) 383–392.

[32] H. Du, A Reevaluation of the Fe-N and Fe-C-N Systems, J. Phase Equilibria. 14 (1993) 682–693.

[33] T. Woehrle, H. Cinaroglu, A. Leineweber, E.J. Mittemeijer, Fe–N and Fe–N–C phase equilibria above 853 K studied by nitriding/nitrocarburising and secondary annealing, Int. J. Mater. Res. 107 (2016) 192–202.

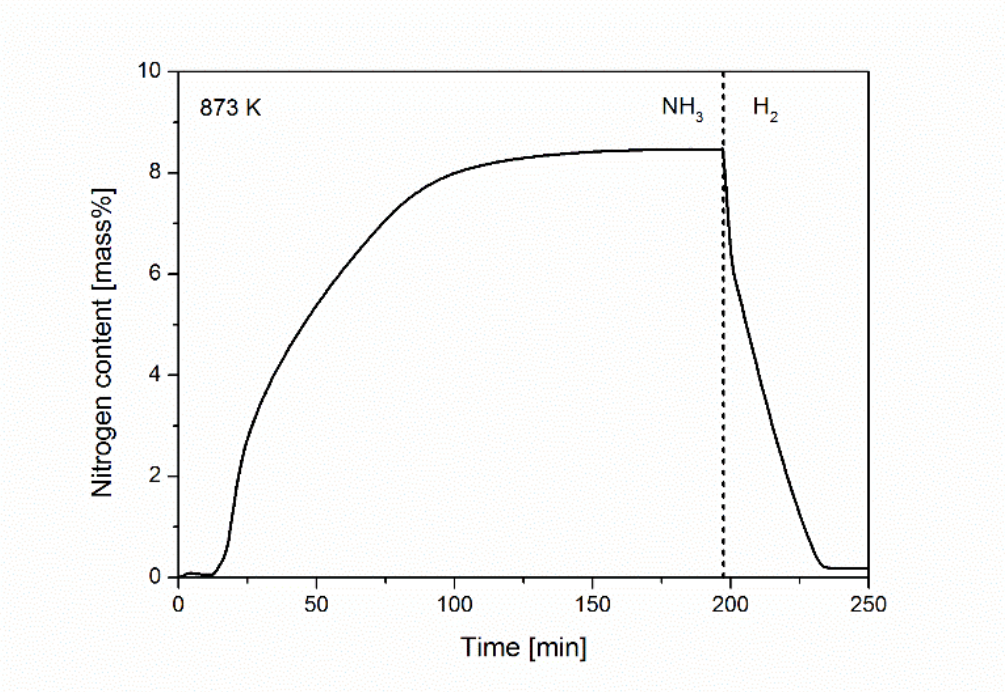

Fig. 1: Thermogravimetric curve for gaseous pretreatment of 25 µm iron foil at 873 K in two steps; nitriding in ammonia (infinite nitriding potential) and denitriding in hydrogen (zero nitriding potential). The apparent difference in initial and final mass is the result of buoyancy effects due to changing temperature and gas composition.

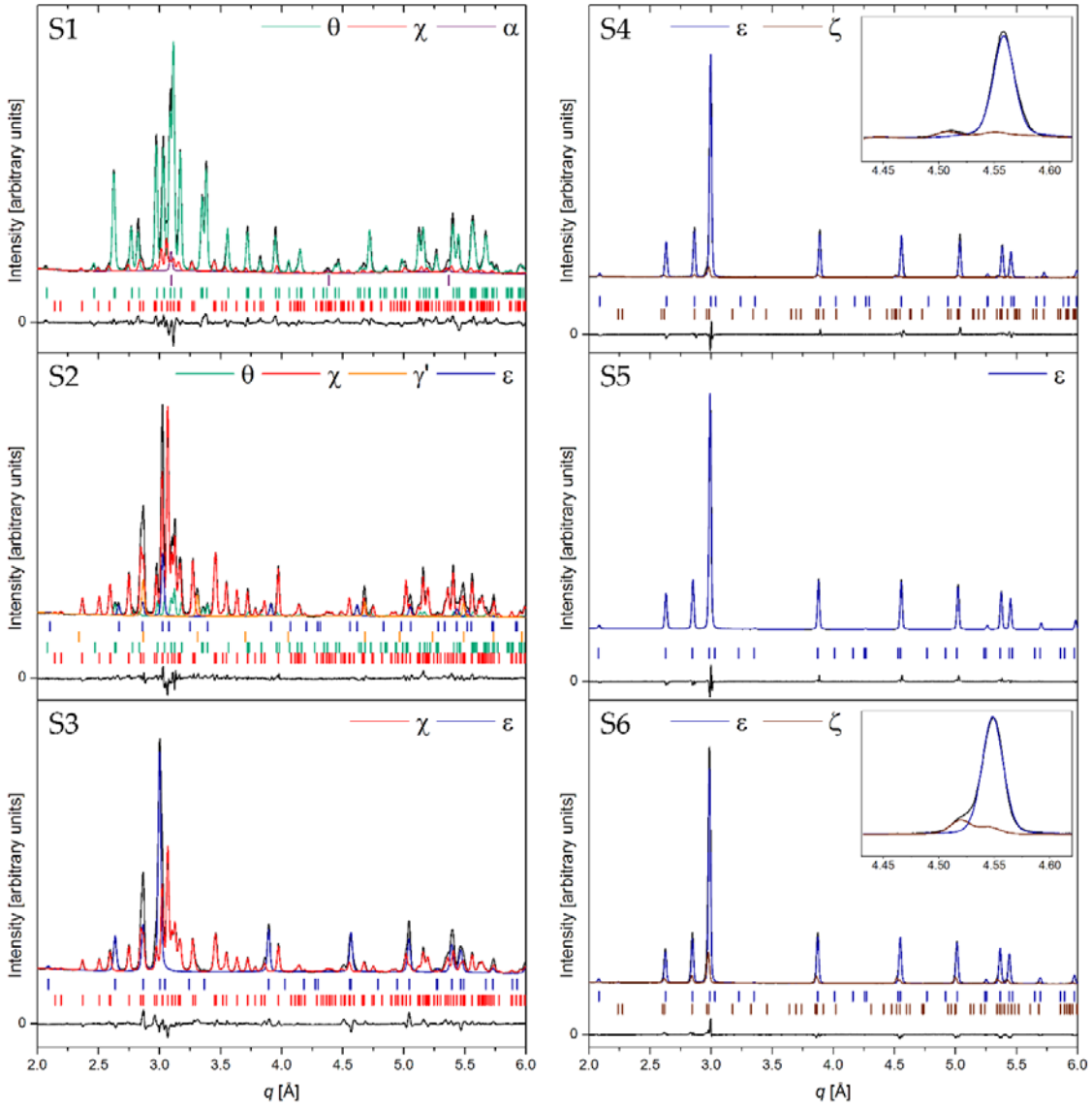

Fig. 2: X-ray diffractograms, refined Rietveld profiles and difference curves up to q = 6.0 $Å^{-1}$ for nitrocarburized porous iron foil. Insets show peaks of two distinct phases, ε and ζ. Profile residuals (R_p) and goodness-of-fit values (χ^2) are ≤ 2.52% and 2.51, respectively.

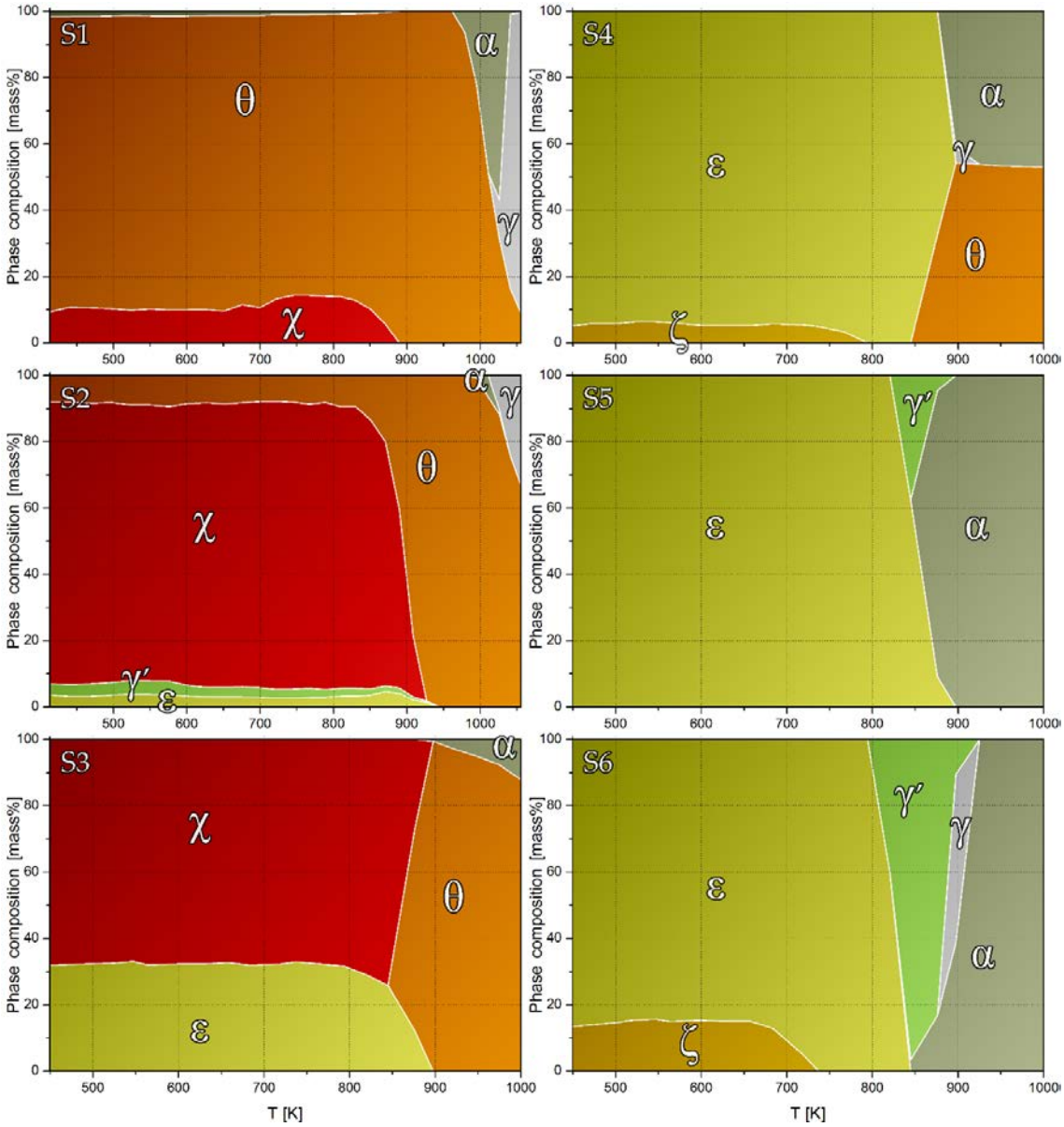

Fig. 3: Phase transformation maps, i.e. phase composition versus temperature, for samples S1-S6. Note the higher temperature range for S1 and S2. Estimated standard deviations from refinements are ≤ 1.1 mass%.

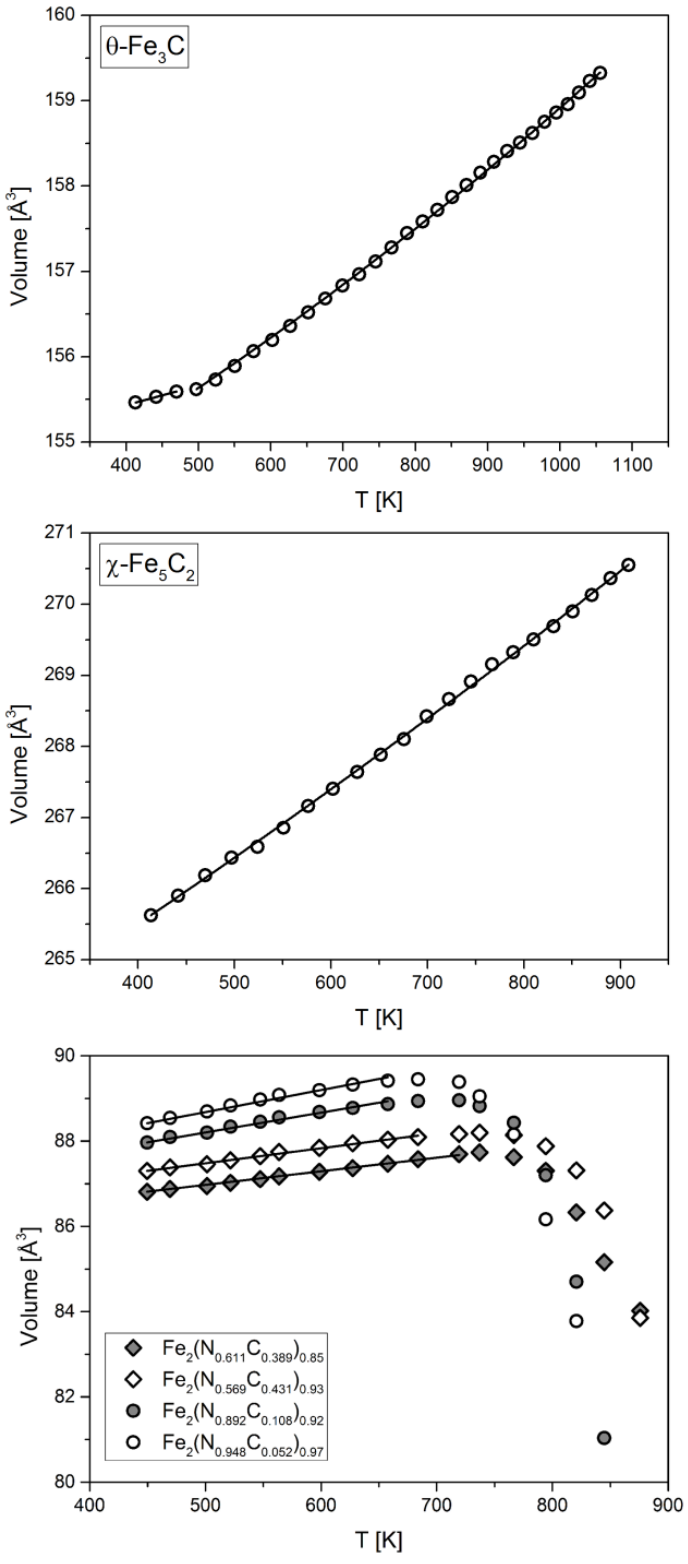

Fig. 4: Unit cell volume versus temperature for cementite (top), Hägg carbide (middle) and ε-$Fe_2(N,C)_{1-z}$ (bottom). Estimated standard deviations are ≤ 0.1 Å^3. Lines correspond to fitted expressions for thermal expansion (equations 1 and 2).

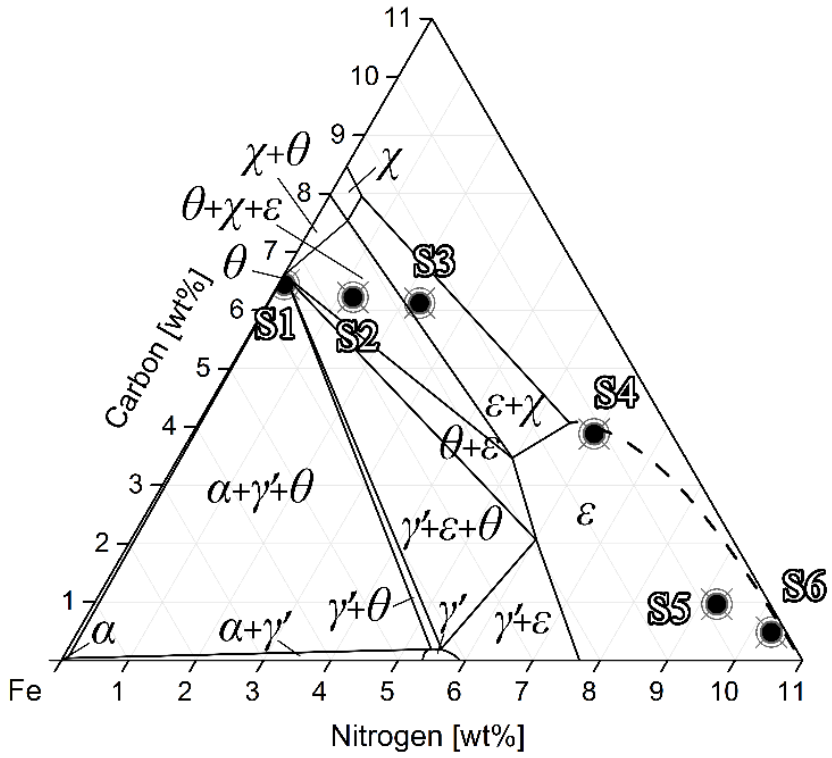

Fig. 5: Compositions corresponding to the six samples prepared at 718 K plotted on the isothermal section of the Fe-C-N phase diagram at 773 K[7].